Structural studies of a Ti–Zr–Ni quasicrystal-forming liquid

Structural studies of a Ti–Zr–Ni quasicrystal-forming liquid

T H Kim[1], G W Lee[2], A K Gangopadhyay[1], R W Hyers[3], J R Rogers[4], A I Goldman[5] and K F Kelton[1]

[1] Department of Physics, Center for Materials Innovation, Washington University, St Louis, MO 63130, USA
[2] Korea Research Institute of Standards and Science, Daejon, Republic of Korea
[3] University of Massachusetts, Amherst, MA 01003, USA
[4] NASA Marshall Space Flight Center, Huntsville, AL 35812, USA
[5] Ames National Laboratory, USDOE and Department of Physics and Astronomy, Iowa State University, Ames, IA 50011, USA

Abstract

Employing the technique of electrostatic levitation coupled with high-energy x-ray diffraction, $Ti_{39.5}Zr_{39.5}Ni_{21}$ liquids were shown previously to develop significant short-range icosahedral order with supercooling. However, that conclusion was based on the assumption of a single dominant cluster type in the liquid and the observed evolution of the high-q shoulder on the second peak in the structure factor, $S(q)$. Here, new diffraction data that were obtained using more rapid data acquisition methods are presented. These allow structural studies to be made down to and through recalescence to the icosahedral quasicrystal. The liquid structures obtained from a Reverse Monte Carlo analysis of these data are characterized by their bond-angle distributions, Honeycutt and Andersen indices and bond orientational order parameters. These analyses indicate that while there are several different types of local order, the icosahedral short-range order is dominant and increases gradually with supercooling.

1. Introduction

The structures of liquids are linked to the phase transitions that occur within them. In 1724 Fahrenheit first observed the tendency of water to resist crystallization when it is cooled below its equilibrium melting temperature [1]. While water is in many ways a unique liquid, this ability to supercool without crystallization is ubiquitous. In the 1950s Turnbull demonstrated that even metals, where the densities and atomic coordination numbers in the liquid and solid phases are almost the same, can be deeply supercooled. To explain this, Frank proposed that the structures of supercooled metallic liquids are dominated by icosahedral short-range order (ISRO), an energetically preferred local structure. Since icosahedral order is incompatible with long-range periodicity, this provided a structural basis for the observed barrier to the nucleation

of the stable ordered phase. To form the crystal phases the icosahedral order must be replaced by the tetrahedral and octahedral configurations of the close-packed structures, requiring that the local structure first transition through higher-energy configurations. Icosahedral order has been identified in many computer simulations of liquids [2, 3] and glasses [4, 5], but only recently has experimental evidence for this been obtained.

The discovery in 1984 of a new phase of condensed matter, the icosahedral quasicrystal, which has the long-range order typical of a crystal phase, but with an icosahedral rotational point group symmetry that is forbidden for a periodic structure, opened the door for novel investigations of the nature of liquid and crystal structures [6]. Like metallic liquids, the structures of metallic glasses are also often assumed to be dominated by icosahedral order. In support of this view, Holzer and Kelton [7] first demonstrated that the interfacial free energy between the i-phase and an Al–Cu–V metallic glass of the same composition was extremely small, indicating that the local atomic structures of the two phases were alike. Similar studies in metallic liquids have proven more difficult, partly because heterogeneous nucleation on the container walls frequently limits supercooling, making it difficult to probe the more fundamental homogeneous nucleation processes. However, a variety of techniques have recently been developed that eliminate the need for a container. These are primarily based on acoustic [8], aerodynamic [9], electrostatic (ESL) [10, 11] or electromagnetic (EML) [12] levitation methods. ESL and EML are the most versatile, allowing simultaneous measurements of the amount of supercooling, liquid structure and thermophysical properties. Using these techniques Holland-Moritz [13] and others [14] have shown that liquids for which the i-phase is the primary nucleating phase have the least undercooling, i.e. like the glass crystallization studies they show a low nucleation barrier due to local icosahedral order in the liquid.

While such investigations support the hypothesis that an increased degree of polytetrahedral order lowers the interfacial free energy between the crystallizing phase and the supercooled liquid thus increasing the nucleation rate, they do not prove it. A proof requires that a significantly decreased barrier for the nucleation of an i-phase in a liquid be measured simultaneously with demonstrated icosahedral short-range ordering. Following that approach, Frank's hypothesis was confirmed recently by combining the ESL technique with high-energy diffraction measurements of Ti–Zr–Ni quasicrystal-forming alloys during supercooling [15]. *In situ* synchrotron x-ray diffraction studies on electrostatically levitated molten droplets of $Ti_{39.5}Zr_{39.5}Ni_{21}$ showed that the i-phase was the primary nucleating phase. However, the i-phase transformed quickly to a C14 polytetrahedral Laves phase, indicating that it was metastable in this temperature range. From simultaneous x-ray diffraction measurements, a shoulder on the high-q side of the second peak in the x-ray structure factor of the liquid that is characteristic of icosahedral order became more pronounced with decreasing temperature. The tetrahedral structure of the C14 phase is also similar to the short-range order of the liquid and the C14 is known to nucleate easily over a wide composition range. The preferential crystallization of the liquid to the i-phase, which has a lower driving free energy (since it is metastable at that temperature), demonstrates that the nucleation barrier for the i-phase was less than that for crystallographic phases, even for those with local polytetrahedral order. The correlation between ISRO and the nucleation barrier confirmed Frank's hypothesis. Subsequent BESL studies of elemental transition liquids have also demonstrated the growth of ISRO with supercooling. The ISRO is more distorted in the early transition metals, however, likely reflecting a competition between close packing to maximize density and the angular dependence of the transition metal bonding [16].

The earlier liquid structural studies assumed that the liquid structure could be described by a single dominant cluster type. Not surprisingly, more recent studies of the elemental transition metal liquids using Reverse Monte Carlo methods to obtain a structure have shown

there are actually several significantly different local environments [17]. The RMC studies have, however, confirmed that ISRO is in many cases the most dominant structural type. In this paper, we report the results of a RMC analysis of the Ti–Zr–Ni liquid structures from new x-ray diffraction data. These results support the previous results of the dominant ISRO character in the structures of these quasicrystal-forming liquids but a range of other types of local structures are also found. Before discussing these results it is useful to discuss the BESL method (Beamline ESL) for obtaining the scattering data and the methods of analysis.

2. Experimental procedures

The ESL technique has several advantages over EML methods; sample heating is decoupled from sample levitation and samples are not limited by their electrical conductivity, allowing a wide range of samples to be processed [10, 11]. The only limiting factor is the sample vapor pressure, which should be less than approximately 10 mTorr. In ESL charged samples with a 2.0–3.0 mm diameter (approximately 30–70 mg mass) are levitated by Coulomb forces in an electrostatic field (0–2 MV m^{-1}) under high vacuum ($\approx 10^{-7}$ Torr). Three pairs of orthogonal electrodes control the sample position during processing to within 50–100 μm using active feedback control based on error signals from two orthogonal position-sensitive detectors. The samples are initially charged by induction and the charge is maintained during processing with an external UV source. The levitated samples are heated with a diode and/or a CO_2 laser and the sample temperature is measured with optical pyrometers (Mikron Infrared, Inc.) operating in a 1.45 and 1.8 μm wavelength range.

Recently we modified the ESL to make structural measurements on supercooled levitated liquids [15, 18]. The ESL chamber was mounted on an Eulerean cradle on beamline 6ID-D of the MU-CAT facility at the Advanced Photon Source (APS) located at Argonne. The height of the cradle was adjusted so that the center of the sample was coincident with the center of the incident beam. Measurements were made in a transmission geometry using high-energy (125 keV, 0.099 Å) x-rays. The x-ray beam entered the chamber through a 2.5 inch diameter and 0.015 inch thick Be window and the scattered beam exited through a 4 inch diameter Be window that was located on the opposite side of the chamber to the entrance window. A MAR3450 image plate (Fuji Photo Film Co. Ltd) and a GE-Angio 41 cm area detector (model 2304879, manufactured by PKI Inc. for GE Inc., Milwaukee) were used to rapidly obtain complete diffraction patterns over a wide momentum transfer range (0.5 Å^{-1} $\leqslant q \leqslant$ 15 Å^{-1}). The studies reported here were made with the GE detector using acquisition rates of up to 30 complete diffraction patterns per second. This allowed a continuous measurement of the structural evolution of the supercooled liquid through crystallization.

The diffraction data from the area detector were integrated using the *fit2D* program [19] to obtain diffraction patterns as a function of scattering wavevector. Corrections to those data were made for background scattering from air, the Be windows of the chamber and a minor background correction for scattering within the chamber, absorption effects (minimal), multiple scattering (minimal), and Compton scattering contributions using the *PDFGETX2* [20] analysis package. Due to the highly polarized nature of the synchrotron beam and the small scattering angles used in the present studies, polarization corrections were negligible. The background corrections were determined from measurements of a polycrystalline Si (NIST standard). The pair correlation function, $g(r)$, was computed from $S(q)$ as

$$g(r) = 1 + \frac{1}{4\pi r \rho_0} \left[\frac{2}{\pi} \int_0^\infty q \left[S(q) - 1 \right] \sin(qr) \, dq \right], \tag{1}$$

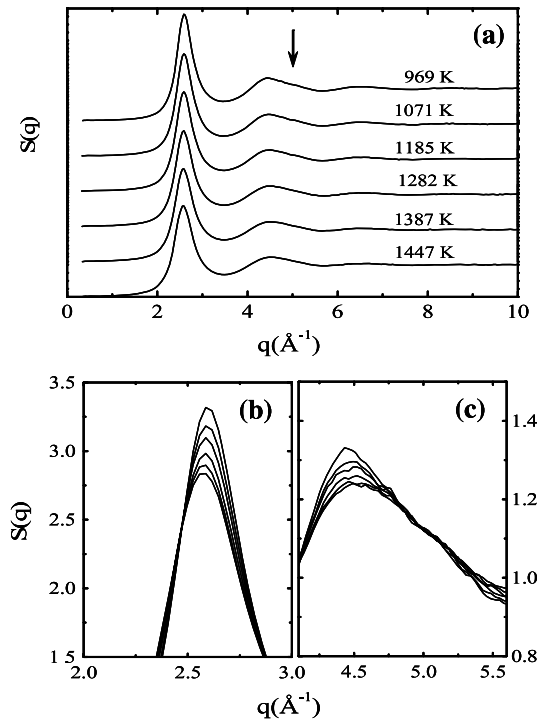where ρ_0 is the average number density (atom Å^{-3}). The coordination number, N, of the first

3

Figure 1. (a) Structure factor, $S(q)$, for a $Ti_{39.5}Zr_{39.5}Ni_{21}$ liquid obtained from diffraction patterns taken at a frame rate of 1 Hz during cooling. The arrow indicates the location of the shoulder on the second peak. Enlarged view of the first peak (b) and the second peak (c) at the same temperature as in (a) showing the increased intensities with cooling.

shell was obtained by integrating the radial distribution function (RDF $= 4\pi r^2 \rho_0 g(r)$) up to the first minimum after the main peak.

3. Experimental results

Figure 1(a) shows the measured x-ray structure factors, $S(q)$, as a function of temperature for supercooled liquid $Ti_{39.5}Zr_{39.5}Ni_{21}$. The evolution of the peaks of $S(q)$ during supercooling indicates ordering in the liquid with decreasing temperature.

The arrow in the figure indicates a shoulder on the second peak in $S(q)$ that becomes more prominent with increased supercooling due to an increasing intensity of the second peak (figure 1(c)). The intensity of the first peak also increases (figure 1(b)). The position of the first peak remains constant with supercooling while that of the second peak moves to lower q. The relative locations of the high-q shoulder on the second peak in $S(q)$ and the first and second peak positions are close to those for a perfect icosahedron [21] and become closer with supercooling, in agreement with the results of an earlier cluster-based analysis of the $S(q)$ [15].

The reduced radial distribution function, $G(r)$, computed from the experimental $S(q)$

$$G(r) = \frac{2}{\pi} \int_0^\infty q \left[S(q) - 1 \right] \sin(qr) \, dq \tag{2}$$

is shown as a function of temperature in figure 2(a), with enlarged views in figures 2(b) and (c). The first peak sharpens during supercooling while the peak position remains unchanged. The second peak position moves to lower r, while also slightly sharpening. The sharpening indicates better order; that both peak positions do not change with cooling indicates that the changes in the second peak position are not due to thermal expansion but to changes in the nearest-neighbor environment.
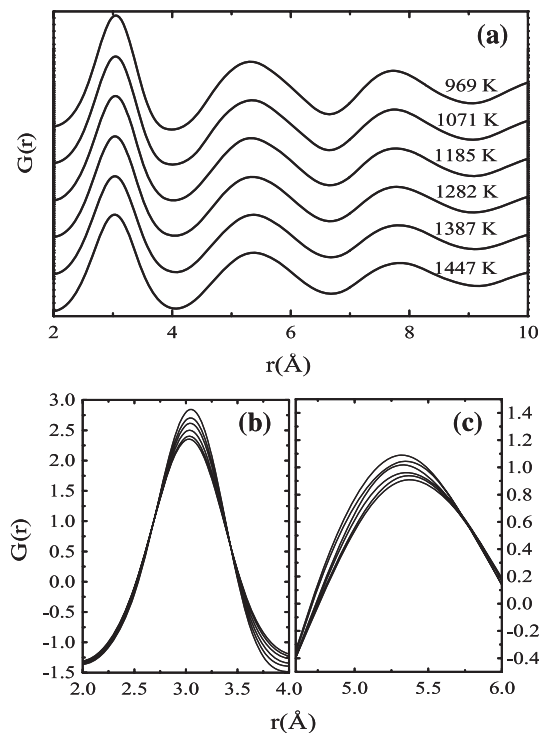
Figure 2. (a) Reduced radial distribution functions $G(r)$ for a $Ti_{39.5}Zr_{39.5}Ni_{21}$ liquid. Enlarged views of (b) the first peak in $G(r)$ (b) and (c) the second peak for the same temperatures as in (a) (data taken at rate of 1 Hz during cooling). The intensity of both increase with increased cooling. Note the almost constant location of the first peak along and the shift of the second peak toward smaller distance.
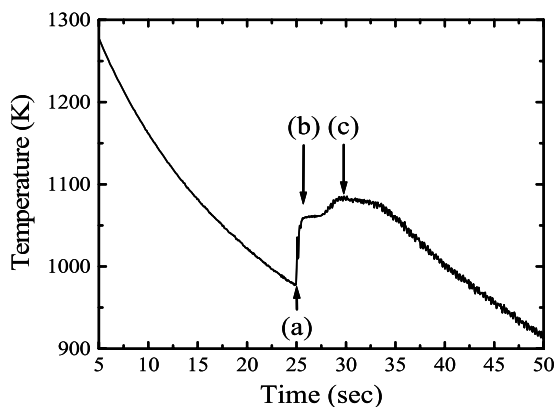

Figure 3. The cooling curve for $Ti_{39.5}Zr_{39.5}Ni_{21}$ alloy as a function of time: (a) primary recalescence, (b) metastable melt plateau, (c) secondary recalescence.

Diffraction patterns were measured at a frame rate of 30 Hz (33 ms per pattern) as the sample was allowed to cool by radiative cooling with no laser heating. The temperature of the sample during cooling is shown in figure 3. Two different recalescence events are noticed; the first recalescence, the first plateau and the second recalescence are indicated by the arrows (a), (b) and (c) respectively. The corresponding diffraction patterns are shown in figure 4. These results confirm those reported earlier by Kelton *et al* using the slower MAR3450 image plate. The primary crystallizing phase (first recalescence) is an icosahedral quasicrystal phase (*i*-phase). The second recalescence corresponds to a phase transition to the stable C14 Laves phase. The short lifetime of the *i*-phase indicates that it is metastable at this temperature, in agreement with phase diagram studies [22]. No abrupt changes in $S(q)$ or
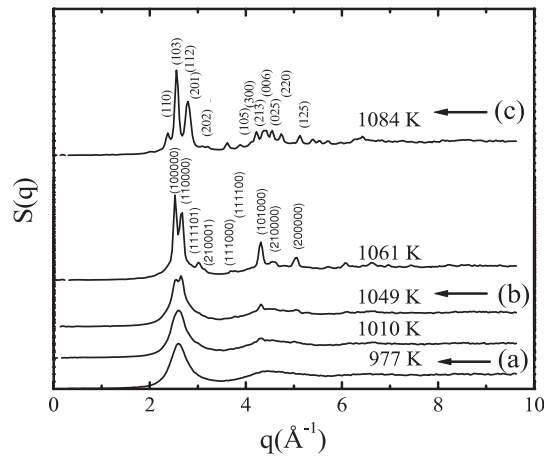
Figure 4. Structure factors from the time resolved diffraction measurements (33 ms per pattern) for Ti$_{39.5}$Zr$_{39.5}$Ni$_{21}$ alloy. The arrows (a), (b) and (c) indicate the onset of the 1st recalescence, the 1st plateau and the 2nd recalescence. The crystal peaks corresponding to the *i*-phase and the C14 phase are listed.

Table 1. Density (ρ), simulation cube size (L) and cutoff distance applied for various simulation temperatures for simulations of Ti$_{39.5}$Zr$_{39.5}$Ni$_{21}$, along with the melting temperature.

T (K)	ρ (Å^{-3})	L (Å)	Cutoff (Å)	T_{m} (K)
969	0.0539	45.2	2.0	1083
1071	0.0536	45.4	2.0	
1185	0.0530	45.5	2.0	
1282	0.0525	45.7	2.0	
1387	0.0520	45.8	2.0	
1477	0.0516	45.9	2.0	

the coordination number were observed before recalescence, indicating that order in the liquid develops continuously with no sudden change prior to crystallization.

4. Discussion

The previous analysis of such data was based on an isolated cluster modeling. To obtain a more detailed description of the structural evolution with supercooling a Reverse Monte Carlo (RMC) [23–25] technique was used to analyze the $g(r)$ obtained from these new data. 5000 atoms were placed in a cube of side $L = 45.2$–45.9 Å, depending on the temperature of the system. Several structures below and above the melting temperature (1083 K) were simulated, using the appropriate experimental number densities. Table 1 lists the densities and temperatures that were simulated. In addition to these parameters, 6 cutoff distances are required for a 3 component alloy to define the distance of minimum approach for each possible pair of neighboring atom species: AA, AB, AC, BB, BC and CC. This distance was determined to be 2.0 Å from the first minimum in the pair correlation function.

The experimental $g(r)$ and that the RMC fits are in good agreement (figure 5). In the following discussion, only the atom positions and not their chemistry are considered. The distribution of bond angles calculated between a central atom and two nearest-neighboring atoms, is often used to evaluate RMC structures. In terms of dominant clusters the bond
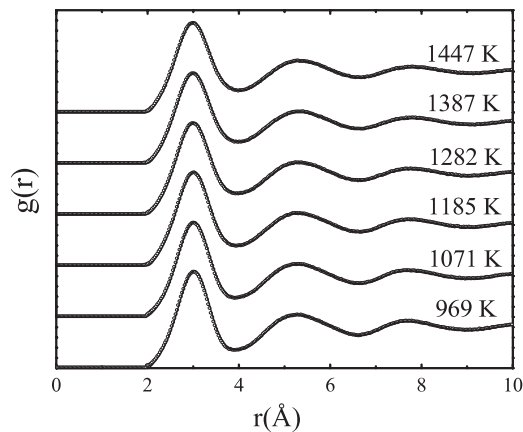
Figure 5. The $g(r)$ curves as a function of temperature for the $Ti_{39.5}Zr_{39.5}Ni_{21}$ liquid: (solid lines) $g(r)$ calculated from the RMC fit structures and (circles) and $g(r)$ obtained from the experimental diffraction data (taken at a rate of 1 Hz during cooling).
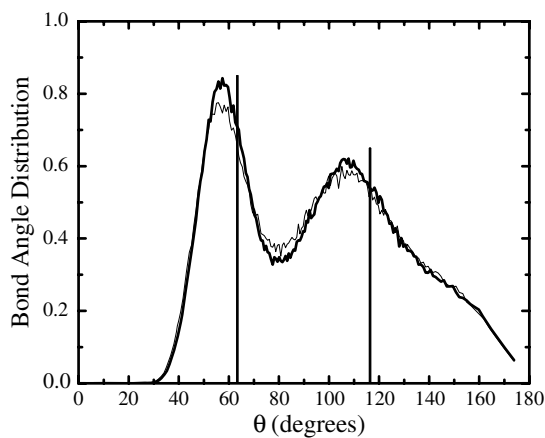

Figure 6. The bond-angle distribution for $Ti_{39.5}Zr_{39.5}Ni_{21}$ liquids at different temperatures. The thick line indicates the distribution of the structure at the lowest temperature (969 K) and the thin line is that at 1447 K. Though intermediate temperatures are not shown, the intensity of the distribution increases continuously with cooling. The vertical lines indicate the bond angles for perfect icosahedral order.

angles characteristic of icosahedral order are $63.4°$ and $116.4°$ while the prominent angles for crystallographic fcc, hcp and bcc clusters are $60°$, $90°$ and $120°$. Figure 6 shows this distribution for the $Ti_{39.5}Zr_{39.5}Ni_{21}$ liquid at the highest and lowest temperatures measured; the peak positions are approximately $57°$ and $106°$, with an estimated error of less than $3°$. The vertical lines correspond to the expected angles for icosahedral order. While they are close to the peak positions determined from the RMC fits, closer than the crystallographic angles (note the absence of $90°$), they are not in good agreement, suggesting that either the icosahedral order is distorted or there is a significant presence of other local structures. The bond-angle distribution intensity increases with cooling, indicating ordering, and the peaks shift slightly to higher angles, consistent with an increase in icosahedral ordering.

Honeycutt and Andersen (HA) indices [26] and bond orientational order parameters (BOO) [2, 27] were used to obtain a more quantitative measure of the RMC structures. The (HA) indices provide topological information. In this method each pair of atoms in the cluster is taken in turn as a root pair, and the local structure around this pair is described by four indices. The indices denote the following: (1) to which peak in $g(r)$ the pair belongs; (2) how many atoms are counted as nearest neighbors of the root pair; (3) the number of pairs of these nearest neighbors that are close enough to form a bond; (4) a classification for clusters with identical sets of the first three indices, but with different bond arrangements. A more complete discussion is provided elsewhere [26]. It is important to note that a leading index of 1 refers
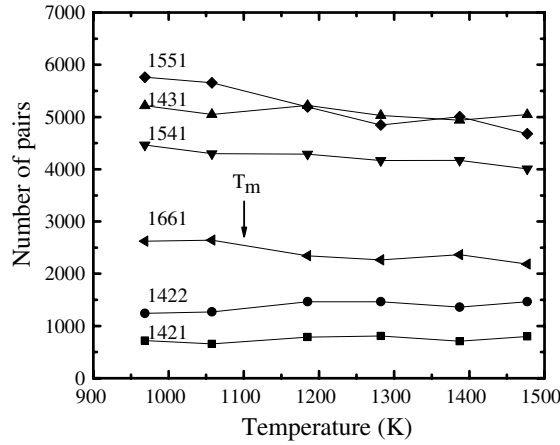
Figure 7. HA indices as a function of temperature calculated from the fit RMC structures for $Ti_{39.5}Zr_{39.5}Ni_{21}$ supercooled liquids. With supercooling, the number of indices associated with icosahedral order (1551, 1541 and 1431) and bcc order (1661) increase. The indices associated with fcc and hcp order (1421 and 1422) do not change significantly.

to first nearest neighbors and a leading index of 2 to second nearest neighbors. Also, some indices are more prominent for particular structures. For example, the 2211, 2101, 1421 and 2441 indices are characteristic of a FCC structure; HCP structures contain these indices, but the 1422 and 2331 are also prominent. The 1441, 1661, 2101, 2211, and 2441 indices are characteristic of the bulk BCC structure and the 1551 and 2331 indices are characteristic of an icosahedral structure. Structures with distorted icosahedral order have a high density of 1431 and 1541 indices (see [17] and references therein). The number of each of these indices that is counted indicates the degree of each specific type of ordering. As will be shown, this analysis supports the assertion made previously [15] that the dominant order in $Ti_{39.5}Zr_{39.5}Ni_{21}$ liquids is icosahedral, though various other types of local order were also inferred.

The BOO parameter analysis provides additional information on the changes that occur with increased supercooling. A set of order parameters expressed in terms of spherical harmonics, $Q_{lm}(\boldsymbol{r}) = Y_{lm}(\theta(\boldsymbol{r}), \varphi(\boldsymbol{r}))$, are associated with the orientation of each pair of atoms. To account for equivalent structures that are oriented differently, the rotationally invariant combination is used:

$$Q_l = \left[\frac{4\pi}{2l+1} \sum_{m=-l}^{l} |\overline{Q}_{lm}|^2 \right]^{1/2}. \tag{3}$$

Different structures are characterized by Q_l's of different intensities. For example, cubic symmetry is identified by having a first non-zero value of Q_4, whereas for icosahedral structures Q_6 is the first non-zero value. Since the values of the Q_l's depend of the number of bonds, the Q_l's determined from the experimental liquid data were normalized with respect to the Q_l's for a completely random system. Note that an isotropic structure gives zero values for all Q_l's.

Figure 7 shows the results of the HA index analysis. Consistent with the results of the bond-angle distribution analysis, the structure is not characterized by a single type of local order, but several different ones. The indices for icosahedral (1541, 1431 and 1551) and bcc order (1661) increase gradually during supercooling, whereas the indices for fcc and hcp (1421, 1422) remain constant. Below the melting temperature (1083 K), there is significantly more icosahedral order than above T_m. In addition, the number of icosahedral indices (1551, 1541
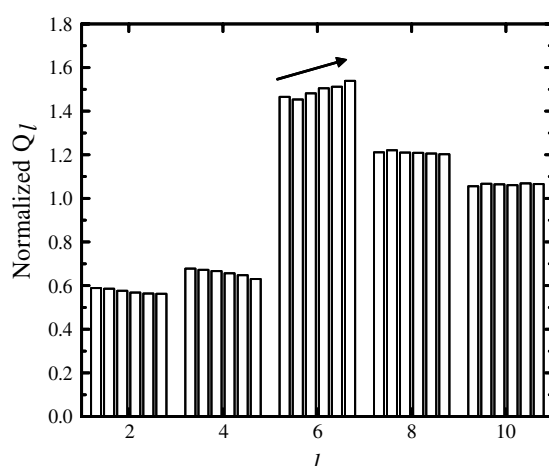
8

Figure 8. Calculated BOO parameters calculated from the fit RMC structures for $Ti_{39.5}Zr_{39.5}Ni_{21}$
supercooled liquids for the temperature shown in figure 7. The arrow indicates the direction of
decreasing temperature. Note that the intensity of the normalized Q_6 parameter (characteristic of
icosahedral order) increases, while the other Q_l's decrease slightly.

and 1431) is almost 3–5 times larger than that of fcc/hcp indices, indicating that the dominant
local structure of the TiZrNi liquid forming an icosahedral quasicrystal is also icosahedral.

The results of the BOO analysis are presented in figure 8. These also indicate icosahedral
ordering with supercooling. The intensity of index 6 (an indicator of icosahedral order) shows
an increase, while those of the other indices decrease. However, the intensity of index 6 does
not reach that of the perfect icosahedron (normalized Q_6: 3.229), again reflecting the existence
of the other types of clusters in the liquid.

All results from the bond-angle distribution, the HA indices and the BOO parameters
indicate dominant icosahedral short-range order in liquid TiZrNi. Lee *et al* have reported that
some systems exhibit a small interfacial free energy between liquid and crystal phase and less
supercooling than that of liquids forming noncomplex crystalline phases [28], in agreement
with the result of these RMC studies. Based on this collection of studies it is clear that the local
structure of the $Ti_{39.5}Zr_{39.5}Ni_{21}$ liquid is very similar to that of the quasicrystals.

5. Conclusions

In conclusion, the evolution of the local structure of liquid $Ti_{37.5}Zr_{37.5}Ni_{21}$ with supercooling
was determined from an analysis of new high-energy x-ray diffraction data obtained from
electrostatically levitated liquid samples. The atomic structures determined from the measured
$S(q)$ by a reverse Monte Carlo fit were analyzed in terms of the bond-angle distributions,
Honeycutt–Anderson indices and bond orientational order parameters. These results indicate
that there is no single local structure that fully describes the liquid structure. However, the
analysis reported here indicates that, in agreement with the previous cluster-based studies of the
diffraction data, icosahedral short-range order is the dominant local structure in these liquids
and that the amount of ISRO increases gradually with supercooling. The growing icosahedral
order lowers the nucleation barrier for the quasicrystal, as if the local structure of the liquid
acts as a template, blurring the distinction between homogenous and heterogeneous nucleation.
The influence of preexisting local order in the liquid, then, is an important ingredient in the
liquid/solid phase transition. While confirming Frank's hypothesis, the local order in the liquid

need not necessarily be identified with interfacial energy. Considering it as a structural order parameter may be a more fundamental way to model the nucleation barrier. Finally, it should be pointed out that while the analysis presented here is more general than the single cluster-based analysis presented earlier, quantitative studies based on molecular dynamics simulations with *ab initio* potentials, as have been made in some transition metal liquids [3, 29–32] are needed to gain a deeper understanding of liquid structures and their evolution.

Acknowledgments

References

[1] Fahrenheit D B 1724 *Phil. Trans. R. Soc.* **39** 78
[2] Steinhardt P, Nelson D R and Ronchetti M 1981 *Phys. Rev. Lett.* **47** 1297
[3] Jakse N and Pasturel A 2006 *Mod. Phys. Lett.* **20** 655
[4] He J H and Ma E 2001 *Phys. Rev.* B **64** 144206
[5] Duan G, Xu D, Zhang Q, Zhang G, Cagin T, Johnson W L and Goddard W A 2005 *Phys. Rev.* B **71** 224208
[6] Shechtman D, Blech I, Gratias D and Cahn J W 1984 *Phys. Rev. Lett.* **53** 1951
[7] Holzer J C and Kelton K F 1991 *Acta Metall. Mater.* **39** 1833
[8] Trinh E H and Ohsaka K 1995 *Int. J. Thermophys.* **16** 545
[9] Weber J K R, Hampton D S, Merkley D R, Rey C A, Zatarski M M and Nordine P C 1994 *Rev. Sci. Instrum.* **65** 456
[10] Rhim W-K, Collender M, Hyson M T, Simms W T and Elleman D D 1985 *Rev. Sci. Instrum.* **56** 307
[11] Rhim W-K, Chung S K, Barber D, Man K F, Gutt G A J and Spjut R E 1993 *Rev. Sci. Instrum.* **64** 2961
[12] Herlach D M, Cochrane R F, Egry I, Fecht H J and Greer A L 1993 *Int. Mater. Rev.* **38** 273
[13] Holland-Moritz D 1998 *Int. J. Non-Eq. Process.* **11** 169
[14] Kelton K F, Gangopadhyay A K, Lee G-W, Hannet L, Hyers R W, Krishnan S, Robinson M B, Rogers J and Rathz T 2002 *J. Non-Cryst. Solids* **312–314** 305
[15] Kelton K F, Lee G W, Gangopadhyay A K, Hyers R W, Rathz T J, Rogers J R, Robinson M B and Robinson D S 2003 *Phys. Rev. Lett.* **90** 195504
[16] Lee G W, Gangopadhyay A K, Rathz T J, Rogers J R and Kelton K F 2004 *Phys. Rev. Lett.* **93** 174107
[17] Kim T H and Kelton K F 2007 *J. Chem. Phys.* **126** 054513
[18] Gangopadhyay A K, Lee G W, Kelton K F, Rogers J R, Goldman A I, Robinson D S, Rathz T J and Hyers R W 2005 *Rev. Sci. Instrum.* **76** 073901
[19] Mossa S and Tarjus G 2003 *J. Chem. Phys.* **119** 8069
[20] Qiu X, Thompson J W and Billinge S L J 2004 *J. Appl. Crystallogr.* **37** 678
[21] Sachdev S and Nelson D R 1984 *Phys. Rev. Lett.* **53** 1947
[22] Davis J P, Majzoub E N, Simmons J M and Kelton K F 2000 *Mater. Sci. Eng.* A. **294** 104
[23] McGreevy R L, Howe M A, Keen D A and Clausen K N 1990 Neutron scattering data analysis *Inst. Phys. Conf. Ser.* **107** 165
[24] Keen D A and McGreevy R L 1990 *Nature* **344** 423
[25] McGreevy R L 1991 *J. Phys.: Condens. Matter* **3** F9
[26] Honeycutt J D and Andersen H C 1987 *J. Phys. Chem.* **91** 4950
[27] Steinhardt P J, Nelson D R and Ronchetti M 1983 *Phys. Rev.* B **28** 784
[28] Lee G W, Gangopadhyay A K, Croat T K, Rathz T J, Hyers R W, Rogers J R and Kelton K F 2005 *Phys. Rev.* B **72** 174107
[29] Jakse N and Pasturel A 2003 *Phys. Rev. Lett.* **91** 195501
[30] Jakse N and Pasturel A 2004 *J. Chem. Phys.* **120** 6124
[31] Jakse N and Pasturel A 2005 *J. Chem. Phys.* **123** 244512
[32] Ganesh P and Widom M 2006 *Phys. Rev.* B **74** 134205